Bi©hemistry

pubs.acs.org/biochemistry Article

Elucidation of the Catalytic Sequence of Dihydroorotate Dehydrogenase B from Lactoccocus lactis: Evidence for Accumulation of a Flavin Bisemiquinone State in Catalysis

Corine O. Smith and Graham R. Moran*



Cite This: Biochemistry 2024, 63, 1347-1358



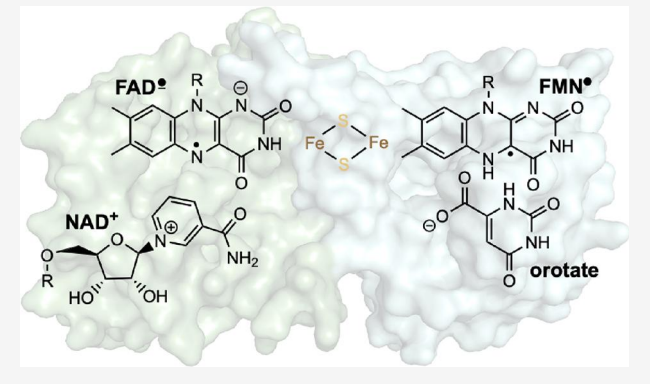
ACCESS I

III Metrics & More

Article Recommendations

Supporting Information

ABSTRACT: The physiological role of dihydroorotate dehydrogenase (DHOD) enzymes is to catalyze the oxidation of dihydroorotate to orotate in pyrimidine biosynthesis. DHOD enzymes are structurally diverse existing as both soluble and membrane-associated forms. The Family 1 enzymes are soluble and act either as conventional single subunit flavin-dependent dehydrogenases known as Class 1A (DHODA) or as unusual heterodimeric enzymes known as Class 1B (DHODB). DHODBs possess two active sites separated by ~ 20 Å, each with a noncovalently bound flavin cofactor. NAD is thought to interact at the FAD containing site, and the pyrimidine substrate is known to bind at the FMN containing site. At the approximate center of the protein is a single Fe₂S₂ center that is assumed to act as a conduit, facilitating one-electron transfers between the flavins. We present anaerobic transient state analysis of a



DHODB enzyme from Lactoccocus lactis. The data presented primarily report the exothermic reaction that reduces orotate to dihydroorotate. The reductive half reaction reveals rapid two-electron reduction that is followed by the accumulation of a fourelectron reduced state when NADH is added in excess, suggesting that the initial two electrons acquired reside on the FMN cofactor. Concomitant with the first reduction is the accumulation of a long-wavelength absorption feature consistent with the blue form of a flavin semiquinone. Spectral deconvolution and fitting to a model that includes reversibility for the second electron transfer reveals equilibrium accumulation of a flavin bisemiquinone state that has features of both red and blue semiquinones. Single turnover reactions with limiting NADH and excess orotate reveal that the flavin bisemiquinone accumulates with reduction of the enzyme by NADH and decays with reduction of the pyrimidine substrate, establishing the bisemiquinone as a fractional state of the twoelectron reduced intermediate observed.

INTRODUCTION

Pyrimidine dehydrogenases are flavin-containing enzymes that catalyze two-electron redox reactions in both pyrimidine biosynthesis and catabolism. The physiological function of dihydroorotate dehydrogenases (DHODs) is the oxidation of dihydroorotate to orotate, the precursor for the de novo biosynthesis of pyrimidine nucleotides. Broadly, DHODs can be divided into Family 1 enzymes that are soluble and typically expressed in lower eukaryotes, archaea, and Gram-positive bacteria and Family 2 enzymes that are membrane associated and produced by eukaryotes and Gram-negative bacteria. The Family 1 enzymes have two oligomeric forms; class 1A enzymes are homodimeric and have a TIM-barrel topology and a noncovalently bound FMN cofactor. The Class 1A enzymes therefore behave as conventional flavin-dependent dehydrogenases in which one active site interacts with oxidant and reductant substrates. These enzymes have unique specific oxidant substrates, such as fumarate.

The class 1B enzymes, the subject of this study, are heterodimers in which one subunit has the structural topology of class 1A enzymes but is associated with a second subunit that has an FAD and an Fe₂S₂ center. The iron-sulfur cluster is positioned between the two flavin isoalloxazine rings and presumably acts as a conduit for electrons² (Figure 1). X-ray crystal structures solved in the presence of orotate verify that the topologically conserved FMN domain has the pyrimidine binding site. For the Class 1B enzymes, the biosynthetic oxidant substrate is NAD+ that is assumed to bind adjacent to the FAD. This cofactor arrangement is reminiscent of that observed in dihydropyrimidine dehydrogenases (DPD) where

Received: January 16, 2024 April 18, 2024 Revised: Accepted: April 19, 2024 Published: May 1, 2024





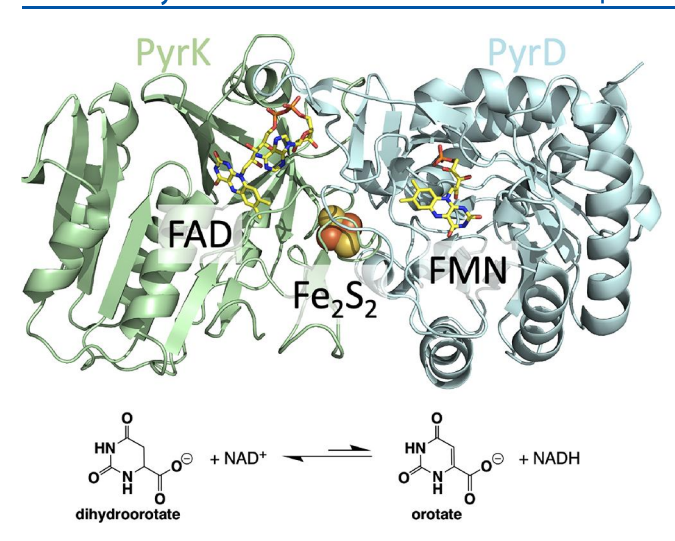


Figure 1. Structure and biosynthetic reaction of DHOD B. Structure figure compiled from PDB 1EP3.

the FAD and FMN are separated by four Fe_4S_4 centers.^{3,4} Interestingly, the FMN containing domain of DPD (domain IV) has the same fold as that observed in the FMN binding domain of family 1 DHODs, indicating a certain modularity to the architecture of pyrimidine oxidoreductases. For DHODB and DPD, the intervening iron—sulfur centers dictate that electrons must pass between the flavins one at a time requiring transient formation of semiquinone forms of both flavin cofactors.

We present an anaerobic transient-state analysis of DHOD 1B from Lactoccocus lactis (LlDHODB). The oxidation of pyrimidine substrates is energetically disfavored, and as such we have primarily characterized the pyrimidine reduction chemistry of this enzyme. As predicted from the architecture, the enzyme exhibits separation of the two electrons acquired from NADH for transmittance through the Fe₂S₂ center resulting in the accumulation of a flavin bisemiquinone form. Here, we propose that this phenomenon is only observed as a result of reversibility in the second single-electron transfer, resulting in low fractional accumulation of a state that has two flavin semiquinones simultaneously. That this state of the enzyme arises concomitant with two-electron reduction of the enzyme suggests that electron transfer between the flavins is rapid relative to hydride transfers steps. These data provisionally establish the chemical sequence of DHODB and DPD enzymes first predicted from X-ray crystal structures.²⁻⁴

MATERIALS, METHODS, AND QUANTITATION

Materials. Competent *E. coli* BL21(DE3) cells were purchased from New England Biolabs. FeSO₄, flavin adenine dinucleotide (FAD), imidazole, tryptophan, dihydroorotate, and triethylamine (TEA) were from Acros. The Miller formulation of lysogeny broth (LB) was from RPI. Ampicillin was purchased from Alfa Aesar. Oxidized nicotinamide adenine dinucleotide (NAD⁺) was purchased from Amresco. TALON Superflow resin was obtained from Cytiva. Macro-Prep High Q anion exchange media were acquired from Bio-Rad. Isopropylbeta-D-thiogalactopyranoside (IPTG), glycerol, Na₂SO₄, sodium dodecyl sulfate (SDS), ethylenediaminetetraacetic acid (EDTA), NaCl, trichloroacetic acid (TCA), and orotate were purchased from Fisher. Glucose oxidase and reduced nicotinamide adenine dinucleotide (NADH) were purchased

from Millipore-Sigma. Ferene-S and NaOH were obtained from Sigma-Aldrich. Glucose was purchased from Spectrum Chemical. Flavin mononucleotide (FMN) was purchased from TCI. Nitric acid was from VWR.

Concentrations of enzyme, substrates, and products were determined based on the following extinction coefficients: Lactoccocus lactis DHOD 1B, $\varepsilon_{454}=35,500~{\rm M}^{-1}{\rm cm}^{-1}$ (see below); LIDHODB FMN subunit dimer, $\varepsilon_{452}=11,900~{\rm M}^{-1}{\rm cm}^{-1}$; orotate, $\varepsilon_{278}=6,700~{\rm M}^{-1}{\rm cm}^{-1}$; NAD+, $\varepsilon_{260}=17,800~{\rm M}^{-1}{\rm cm}^{-1}$; NADH, $\varepsilon_{340}=6,220~{\rm M}^{-1}{\rm cm}^{-1}$. All other concentrations were defined by weight for solids or for liquids, the indicated concentration provided by the manufacturer. All concentrations indicated for transient-state experiments are post-mixing.

Cloning, Expression, and Purification. The two genes that code for LIDHODB are pyrD (FMN subunit) and pyrK (FAD, Fe₂S₂ subunit). These genes were synthesized by Genscript, Inc. (Piscataway, NJ) with the codon bias optimized for expression in E. coli. Both genes were subcloned into the plasmid pETDuet-1, to form a construct that expresses both subunits of LlDOHDB. The pyrD gene was synthesized fused to the sequence for an N-terminal 6-His tag (coding for the sequence: MGSSHHHHHHHSQDPNSSSARLQVDKLAA) and subcloned into the NcoI and HindIII restriction sites. The PyrK gene was subcloned into the NdeI and XhoI sites. The resulting plasmid, pLIDHODB, was transformed into competent BL21(DE3) E. coli cells and spread onto LB agar plates with 100 μ g/mL ampicillin selection and grown for 16 h at 37 °C. A single colony was used to inoculate ~20 mL of sterile LB with 100 μ g/mL ampicillin selection. Cells were grown at 37 °C with shaking at 220 rpm until the first sign of turbidity. The culture was aliquoted (600 μ L) and mixed with 0.22 μ m filtered 50% glycerol (400 μ L) and stored at -80 °C.

To express LlDHODB, cell stocks were thawed and spread on LB agar plates (100 μ L per plate, 1 plate per liter of broth) containing 100 μ g/mL ampicillin. The plates were incubated at 37 °C for 14–16 h. The cell lawn was resuspended using ~5 mL of room temperature LB per plate and used to inoculate 2 L baffled Erlenmeyer flasks each containing 1 L of LB with 100 μ g/mL ampicillin. These cultures were incubated at 37 °C with shaking at 220 rpm and grown to an optical density of 0.6 at 600 nm before the temperature was lowered to 25 °C and the culture was allowed to equilibrate for 1 h. Expression was induced with the addition of 100 μ M IPTG, at which time 200 μ M FeSO₄ and 1 mM Na₂SO₄ was also added. The cultures were maintained at 25 °C with shaking at 220 rpm for 22 h prior to harvesting by centrifugation at 3,500g for 40 min.

Unless otherwise indicated, all purification procedures were undertaken at 4 °C. The supernatant was discarded, and the cells were resuspended in 20 mL per liter of culture of ice-cold 50 mM NaPi, 10 mM imidazole, pH 7.4. The cell suspension was placed in a stainless-steel beaker that was seated in an ice/ water slurry. Sonication using a Branson sonifier set to 40 W was used to lyse the cells with 3 bursts of 2 min, each separated by 1 min for temperature equilibration. Lysed cells were centrifuged at 10,000g for 45 min to remove insoluble material prior to loading onto a 10 mL BD TALON column preequilibrated with 50 mM NaPi, 10 mM imidazole, pH 7.4. The column was washed with 100 mL of the same buffer prior to eluting the enzyme with a 400 mL linear gradient to 100% 50 mM NaPi, 200 mM imidazole, pH 7.4, and the elution was collected as 5 mL fractions. The broad peak obtained was pooled and diluted 4-fold with 50 mM NaPi, pH 7.4. The sample was loaded onto a Macro Prep High Q anion exchange column (2.5 \times 12 cm) at 2 mL per min and washed with 200 mL of 50 mM NaPi, pH 7.4. The LlDHODB components were chromatographed and eluted with a 400 mL gradient to 50 mM NaPi, 300 mM NaCl, pH 7.4 and collected as 5 mL fractions. The two peaks were obtained and pooled separately and buffer exchanged into 50 mM NaPi, pH 7.4 using 15 mL Amicon 10 kDa centrifugal filters. The two forms of overexpressed protein were identified as the native form of DHODB and a dimer of the PyrD subunit presumably resulting from excess expression of the *pyrD* gene (see below). Both fractions were stored as 100 μ L aliquots at -80 °C. All experiments were undertaken in 50 mM NaPi, pH 7.4 at 10 °C.

Cofactor Analysis. LIDHODB is reported to have three cofactors FAD, FMN, and an Fe₂S₂ center.² The relative occupancy of FAD and FMN was determined by methods previously reported.8 In triplicate, LIDHODB was diluted into 50 mM NaPi pH 7.4 with the addition of 0.4% SDS and 3 mM EDTA. The sample was heated to 70 °C for 60 min to ensure complete denaturation and release of the bound cofactors. In this mixture, SDS denatures and solubilizes the enzyme and EDTA chelates the liberated iron ions. The resulting solution has visible absorption transitions only from the flavin cofactors. Absorption spectra from 200 to 700 nm were collected before and after the addition of SDS and EDTA and heat denaturation. 1 M KPi, pH 6.5 was added to the sample to precipitate SDS and associated protein prior to HPLC analysis. The sample was centrifuged at 4 °C for 15 min at 10,000g. A Waters X-Bridge C18 column (4.6 \times 250 mm) coupled to a Shimadzu Prominence HPLC system was used to quantify liberated FAD and FMN. The column was equilibrated in 5 mM ammonium acetate with 15% MeOH, pH 6.5. For analysis 10 μ L of the supernatant was injected and chromatographed at 1 mL/min under isocratic conditions in the above buffer. Elution was monitored at 471 and 370 nm. Standard curves for both FAD and FMN were prepared by the same methods to quantify the amount of each cofactor.

Quantification of iron was achieved using the Fe (II) specific chelator ferene-S that forms bidentate associations with Fe(II) ions forming a complex that absorbs strongly at 595 nm. 9-11 Test and control samples were prepared in parallel, where the control sample substituted buffer in place of LlDHODB. In triplicate, LlDHODB (14 μ L of 243 μ M) was added to 100 μ L of 50% nitric acid and heated for 90 min at 70 °C. The sample was cooled to room temperature and neutralized with 91 μ L of 10 M NaOH. A 795 μ L addition of the Ferene-S stock (5 mM Ferene-S, 200 mM ascorbate, 400 mM NH₄CH₃COO pH 4.3) was added, and the mixture was incubated in the dark at room temperature for 17 h. An absorption spectrum of the 1 mL solution relative to the control was collected and the published extinction coefficient of the Fe(II) ferene-S complex (ε_{595} = 35,200 M⁻¹cm⁻¹) was used to determine the concentration of iron in the sample. 10

Ligand Binding. Dissociation constants for nonreducing substrates were based on perturbation of the LlDHODB spectrum with fractional equilibrium occupancy of the substrate binding site(s). For orotate, 1 mL of LlDHODB (9.4 μ M) was titrated with the ligand (0–182 μ M). The spectrum of the sample was recorded after each addition. The largest perturbation of the flavin spectrum occurred at 448 nm and this wavelength was used to define the binding isotherm for orotate. The net change in absorbance at this wavelength

versus concentration of orotate was fit using the quadratic form of the single site binding equation (eq 1). For NAD⁺, 1 mL of LIDHODB (8.9 μ M) was titrated with the ligand (0–160 μ M) and the spectrum was recorded after each addition. Perturbation of the flavin spectrum at 483 nm was used to determine the dissociation constant for NAD⁺ by plotting the change in absorbance at this wavelength versus concentration of NAD⁺. These data were also fit to eq 1. In this equation, [L] is total added ligand, Δ Abs_{max} is the maximum perturbation at the wavelength chosen for analysis, and K_d is the dissociation constant determined.

$$\Delta Abs = \{([L] + \Delta Abs_{max} + K_d) - \sqrt{([L] + \Delta Abs_{max} + K_d)^2 - (4[L]\Delta Abs_{max})} \}/2$$
(1)

Methods Used for Anaerobic Kinetic Analyses.

Anaerobic enzyme samples were prepared in glass tonometers by exchanging gases. Dissolved dioxygen was exchanged for argon gas by cycling between vacuum and low pressure high purity argon 35 times while attached to a Schlenk line. 12 For all reactions residual dissolved dioxygen was removed after exchange cycles by preparing buffers with 1 mM dextrose and the introduction of 1 U/mL glucose oxidase from the tonometer side arm. Substrate solutions were made anaerobic by sparging with high purity argon for 5 min. Similarly, buffers containing substrates were prepared with 1 mM dextrose and glucose oxidase (1 U/mL) was added after sparging and immediately prior to mounting on the instrument. Absorptionbased transient-state measurements were made using a HiTech stopped-flow spectrophotometer (TgK Scientific) equilibrated to 10 °C. Approximately 16 h prior to experimentation, an anaerobic solution containing 50 mM NaPi, 1 mM dextrose,

and 1 U/mL glucose oxidase, pH 7.4 was prepared in a

tonometer, as described above, and drawn into the stopped-

flow instrument to remove residual dioxygen.

The LIDHODB reaction was also characterized using a rapid quench flow instrument under single turnover conditions (RQF-73, TgK Scientific). The RQF was scrubbed of oxygen using a solution of 50 mM NaPi, 1 mM dextrose, and 1 U/mL glucose oxidase for 4 h. A sample of LlDHODB (16 μ M) was made anaerobic as described above and mounted onto the RQF instrument. A substrate solution containing 13 μ M NADH and 47 μ M orotate, and a quench solution containing 1 M TCA and 3 mM EDTA were made anaerobic by sparging and mounted onto the instrument. The substrate solution also contained 25 μ M tryptophan, which served as an inert internal standard for normalization of HPLC chromatogram peak areas. The enzyme and substrate solutions were mixed 1:1 and allowed to react for defined age times (0.004-3 s), after which the solution was mixed 1:1 with the quench solution. Samples were recovered from the instrument and incubated on ice for 15 min before being centrifuged for 15 min at 10,000g to pellet the precipitated protein. The supernatant was collected and stored at -80 °C. Early age times (0.004, 0.007, 0.014 s) were performed in triplicate and later age times (0.04, 0.075, 0.11, 0.4, 3 s) in duplicate. A t_{zero} point was also generated using the same method but with anaerobic buffer in place of the enzyme.

Samples collected from the RQF were analyzed using HPLC. A 20 μ L subsample was injected onto a C18 reverse phase column (Waters XBridge C18, 5 μ m, 4.6 × 250 mm). Quantitation was based on depletion of orotate and accumulation of NAD⁺. These measurements used separate

solvent conditions for each substance. To quantitate orotate, 20 mM TEA, 10 mM ammonium acetate, 1% CH₃CN, pH 6.5 was used. To quantitate NAD⁺ 20 mM TEA, 10 mM ammonium acetate, 2.7% CH₃CN, pH 6.5 was used. For both, elution was performed isocratically at 1 mL/min. The elution was monitored at 220 and 260 nm. Standard curves were generated under the same conditions for NAD⁺ and orotate. All peak areas derived from the HPLC analysis were normalized based on the peak area of the tryptophan internal standard.

Kinetic Data Acquisition and Analysis. Typically, adequate temporal resolution was achieved by collecting data for multiple timeframes. A short period of data collection was used to capture relatively rapid events and a longer period was used to render changes for slower processes. These data were joined together at the limit of the shorter acquisition to form a continuous trace. Single wavelength data were fit analytically using linear combinations of exponential terms (eq 2) or linear combinations of exponential terms added to a straight line (eq 3) using Kaleida Graph software. In these equations, X is the wavelength of observation, A_n is the amplitude associated with phase n, k_{obsn} is the observed rate constant for phase n, t is the time in s, and C is the absorbance end point. Equation 3 has an additional straight-line term (mt) to improve the overall fit for and provide a better measure of the rate constant for the prior phase when slow, noncatalytically relevant drift phases are part of the data captured. For either equation, the rate constants returned are analytical and reflect event time frames and delineation but, in most cases, they do not provide measures of intrinsic rate constants for individual reaction steps as the reactant concentration ratios were in general not pseudo-first order. Dependencies of the observed rate constants (k_{obs}) determined for the reductive-half reaction were fit to the Adair equation (eq 4) to provide an estimate of the limiting rate of reduction (k_{red}) and the dissociation constant for NADH (K_d).

$$A_{Xnm} = \left(\sum_{n=1}^{x} \Delta A_n (e^{-k_{obsn}t})\right) + C \tag{2}$$

$$A_{Xnm} = \left(\sum_{n=1}^{x} \Delta A_n (e^{-k_{obs},t})\right) + mt + C \tag{3}$$

$$k_{obs} = \frac{k_{red}[\text{NADH}]}{K_d + [\text{NADH}]}$$
 (4)

Three dimensional CCD data sets were fit using singular value decomposition (SVD) using the routine available in KinTek Explorer software (KinTeK Corp.). In most cases, the models and estimates for rate constants were selected based on analytical fitting for single wavelength analyses (see above). The models chosen were generally linear multistep irreversible and so use SVD in a functionally similar manner to analytical fitting of single wavelength data to linear combinations of exponentials. Such an approach forces the software to return observed rate constants and deconvolute to yield spectra for delineated states as opposed to modeling all ligand complexes and intermediate states that occur in the reaction. Prior to fitting, each CCD data set incorporated a t_{zero} spectrum (added as a t = 0.00001 s spectrum) compiled from the absorbance contributions of the enzyme and NADH measured for stock solutions during the experiment and using the same detector.

Anaerobic Steady-State Analysis. Anaerobic steadystate kinetic analysis of LIDHODB followed absorption changes that occur with reduction of NAD⁺ or oxidation of

NADH. A sample of LIDHODB (1 μ M) was prepared anaerobically in a tonometer and mixed with anaerobic substrate solutions (0–160 μ M NADH with 180 μ M orotate, $0-160~\mu\mathrm{M}$ orotate with 443 $\mu\mathrm{M}$ NADH, $0-345~\mu\mathrm{M}$ NAD⁺ with 300 μ M dihydroorotate, 0-345 μ M dihydroorotate with 300 μ M NAD⁺). For all assays, the reaction was monitored at 340 nm for 10 s and the initial rate was determined from the linear part of the curve, between 0.2 and 0.4 s. Initial rates were plotted against concentration of pyrimidine or NAD and fit to the Michaelis-Menten equation (eq 5) using Kaleidagraph software. Additionally, apparent $\mathrm{TN}_{\mathrm{app}}/K_{\mathrm{M}}$ values were determined for each substrate by fitting the data to a variation of the Michaelis-Menten equation (eq 6). In these equations, Av. TN_{app} is the apparent average turnover number at a given concentration of substrate. TN_{app} was used in place of the more conventional $v_0/[e]$ or k_{cat} terms as an acknowledgment that the fraction of active enzyme was not established in these

Av.
$$TN_{app} = \frac{TN_{app}[S]}{K_M + [S]}$$
 (5)

Av.
$$TN_{app} = \frac{TN_{app}[S]}{TN_{app}/(TN_{app}/K_M) + [S]}$$
 (6)

DHOD Equilibrium Position. The equilibrium position of the dihydroorotate dehydrogenase reaction was assessed in the forward (DHO and NAD+) and the reverse (orotate and NADH) directions under anaerobic conditions using a variation of the approach used by Beaupre et al.¹³ The experiment monitors the net formation or consumption of NADH at 340 nm with matched concentrations of both the reductant and oxidant substrates. LlDHODB (1 µM) with 1 mM dextrose was prepared anaerobically in a tonometer as described above. All substrate concentrations were 96 μM and were prepared anaerobically as described above. After mixing, absorbance traces were recorded at 340 nm until the changes in absorption ceased (\sim 20 s). The net change in absorbance at 340 nm was used to define the equilibrium position. The data reported are the average of three observations for the forward and reverse reactions.

Stereochemistry of the DHODB Reaction. The stereochemistry of the DHODB reaction was determined using NMR. Solvent deuterium exchange during equilibrium hydride transfer reactions for reductant substrates depleted signals for specific protons revealing the stereochemistry of the reaction for that substrate. This approach takes advantage of protondeuterium exchange at the N5 position of the flavin hydroquinone state. The reactions were carried out under near anaerobic conditions by preparing 1 mL of the substrate solution prepared in NaPi pD 7.8 in D₂O in the body of a tonometer with concentrated LlDHODB (\sim 5-20 μ L) in the side arm. The tonometer was made anaerobic using the methods described above and transferred to a Plas-Laboratories 830 series glovebox. The glovebox was sealed and flushed with pure dinitrogen gas for 35 min and the partial pressure of dioxygen was measured using a Forensics Detectors oxygen meter. After the partial pressure of oxygen inside the glovebox had reached <0.1%, the concentrated enzyme sample was mixed with ~1 mM substrate solution in the tonometer and 0.6 mL was transferred to an NMR tube (final concentration of enzyme 5 μ M). A 500 MHz Bruker Avance NMR system with a cryoprobe was used to collect 1D ¹H

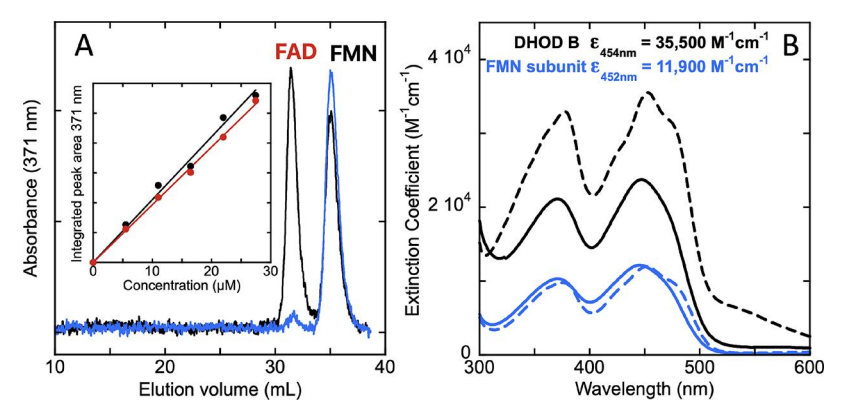


Figure 2. Cofactor quantitation and extinction coefficient determination for LIDHODB. (A) Flavin cofactor determination for DHOD B and the FMN subunit. Flavin cofactors were liberated as described in the methods and quantified by HPLC based on peak area relative to standard curves for both forms of the flavin (inset). The chromatogram for DHOD B is shown in black overlaid with that for the FMN subunit in blue. (B) Extinction coefficients for DHOD B (black) and the FMN subunit (blue) were determined by denaturation with SDS and heating in the presence of EDTA. The known extinction coefficient of the free flavins (solid lines) were used to determine the extinction coefficient(s) of the folded, active states (dashed lines).

spectra. The first FID was acquired approximately 6–8 min after mixing. Spectra were collected automatically over defined period, transforming 32 FIDS for the FMN subunit dimer spectra and 16 FIDS for the LIDHODB spectra.

Calibrated Size Exclusion Chromatography. The pDuet plasmid, pLlDHODB, expressed two stable protein forms and anion exchange separated these components. To establish their structural composition, the molecular weights of both were quantified by calibrated size exclusion chromatography. 1 mL each of five proteins at 10 mg/mL concentration (thyroglobulin (662 kDa), catalase (232 kDa), aldolase (158 kDa), albumin (66.5 kDa), ovalbumin (42.7 kDa)) were chromatographed in pairs to obtain a calibration curve based on the elution volume. The mixtures were loaded onto a 2.5 cm × 100 cm sephacryl S-300 high resolution column preequilibrated with 50 mM NaPi, pH 7.4. Each was eluted at a flow rate of 1 mL min⁻¹. For all standard proteins, the elution volume of each protein was determined using the peak maxima and plotted against its respective molecular weight. The elution volumes were plotted against the log of the molecular weight of the standards and the line obtained was fit to a straight line. The two forms of purified DHODB protein were chromatographed separately in an equivalent manner.

RESULTS

Expression, Purification, and Cofactor Quantitation.

The PyrK and PyrD subunits of LlDOHDB were expressed from the pET-Duet-1 plasmid. This construct favored overexpression of the PyrD subunit (FMN subunit) and so yielded an excess of the His-tagged FMN containing subunit that did not cleanly resolve from the native enzyme during immobilized metal ion affinity chromatography. As a result, the entire colored eluent from the affinity column was pooled and rechromatographed using anion exchange chromatography. This additional step resolved the two expressed proteins (FMN subunit dimer and LIDHODB) (Figure S1). The typical yield per liter of culture was 8 mg for the FMN subunit dimer component and 3 mg for the native LIDHODB component. The identity of these components was established by absorption spectra (Figure 2), activity assay, and calibrated size exclusion chromatography (Figure S2)

Figure 2A depicts quantitation of the flavin content of the two LIDHODB components isolated. These data clearly show that the PyrD sample contains only FMN while the native PyrD:PyrK component contains equal concentrations of both FAD and FMN (FAD:FMN, $1.00 \pm 0.05:0.90 \pm 0.09$). In addition, 1.40 ± 0.01 iron ions per LlDHODB dimer was determined by colorimetric chelation. This ratio of iron ion content suggests that the sample is ~71% constituted with the Fe₂S₂ center. Nonetheless, the enzyme extinction coefficient was calculated based on the FAD, FMN content (Figure 2B). The native LIDHODB component absorption spectrum has additional transitions consistent with the iron-sulfur center that skews the absorption below 380 nm and adds additional broad absorption from 500 to 700 nm. In contrast the FMN subunit dimer component has only absorption transitions consistent with the flavin isoalloxazine ring. These measurements permitted calculation of extinction coefficients for the both isolated components.

Dissociation Constants. Dissociation constants for oxidant substrates were determined by titration, observing perturbation of the DHODB spectrum (Figure 3). Binding of orotate was readily observed and indicted a 10 μ M binding constant. The effect of binding of NAD⁺ on the DHODB spectrum was less apparent inducing small changes in extinction coefficient. The dissociation constant for this ligand was determined to be $\sim 2~\mu$ M.

Steady State. The steady-state parameters for DHODB were measured under anaerobic conditions to avoid observing artificially elevated rates for NADH oxidation resulting from reduced states of the enzyme reducing dioxygen. For each Michealis-Menten curve the concentration of the nontitrated substrate was assumed to be sufficient to be at the zero-order segment of the curve for that substrate and as such these methods return apparent steady-state parameters. The values measured indicate that the orotate reduction reaction is favored over NAD+ reduction. This is reflected both in the turnover number (TN) and the K_m values translating to TN/ K_m values that reveal 10-20-fold substrate preferences for orotate reduction. These values differ markedly from other published steady state parameters measured under aerobic conditions $^{14-16}$ but return ratios of TN/ K_m values for orotate reduction vs NAD+ reduction that agree with the measured reaction equilibrium (see below).

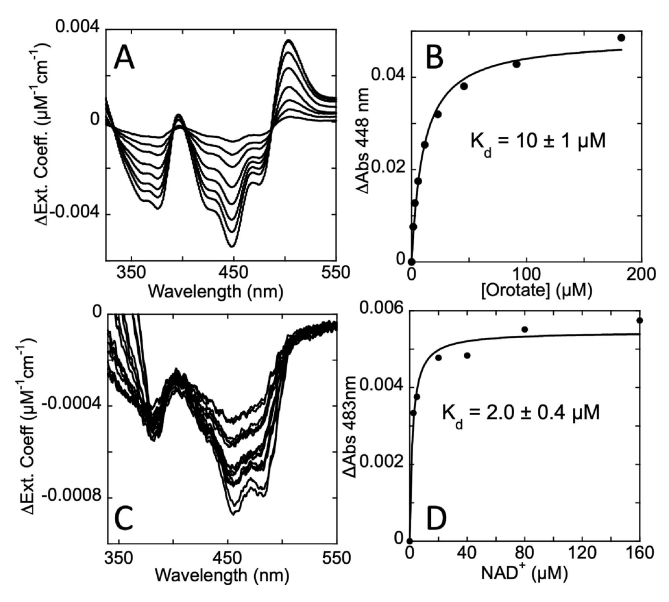


Figure 3. Determination of $K_{\rm d}$ values for orotate and NAD⁺. (A) 1 mL of DHODB (9.4 μ M) was titrated with orotate (0–182 μ M) and the spectrum recorded after each addition. (B) Perturbation of the flavin spectrum at 448 nm was used to determine the dissociation constant for orotate by plotting change in absorbance at this wavelength versus concentration of orotate. These data were fit using the quadratic form of the single site binding eq (eq 1) to yield the value shown. (C) 1 mL of DHOD B (8.9 μ M) was titrated with NAD⁺ (0–160 μ M) and the spectrum recorded after each addition. (D) Perturbation of the flavin spectrum at 483 nm was used to determine the dissociation constant for NAD⁺ by plotting change in absorbance at this wavelength versus concentration of NAD⁺. These data were also fit using the quadratic form of the single site binding equation to yield the value shown.

DHOD Reaction Equilibrium. The equilibrium position for the DHOD reaction was observed directly by combining the enzyme with equimolar concentrations of pyrimidine and NAD and observing the net change in absorbance as the system came to equilibrium. These data indicate that the DHOD reaction favors formation of the DHO by a factor of \sim 9, consistent with the ratio of TN/K_m for the orotate reduction versus NAD⁺ reduction measured in the steady state (Table 1, Figure S3). These data predict a ΔG ° for the orotate reduction reaction of -5.4 kJ/mol.

Table 1. Anaerobic Steady-State Kinetic Parameters for LIDHODB

	NAD ⁺ reduction		orotate reduction	
apparent values	NAD ⁺ (300 μM DHO)	DHO (300 μM NAD+)	NADH (180 μM O)	Ο (443 μM NADH)
$TN (s^{-1})$	5.0 ± 0.2	4.4 ± 0.2	17 ± 1	16.0 ± 0.2
$K_m (\mu M)$	41 ± 5	17 ± 3	7 ± 1	5.7 ± 0.3
$TN/K_{\rm m} \ (\mu M^{-1} \ { m s}^{-1})$	0.12 ± 0.01	0.26 ± 0.04	2.5 ± 0.4	2.8 ± 0.1

Stereochemistry of the DHODB Reaction. The stereochemistry of the DHODB reaction was established using NMR to show exchange of specific protons for deuteriums in equilibrium hydride transfer processes between reducing substrates and the flavins in each of the subunits. The excess expression of the FMN subunit dimer afforded an opportunity to evaluate the stereochemistry of all observed hydride transfer

reactions. This approach takes advantage of the opportunity for solvent exchange of the N5 proton of the hydroquinone form of the flavin isoalloxazine (Figure 4). In deuterated solvent and in the presence of the FMN subunit dimer, dihydroorotate was enriched with deuteriums in both the 5 and 6 positions (Figure 4A). This occurs as there are two opportunities for deuterium exchange in the ligand complex, these being reduction of the FMN with exchange at N5, as described, and reduction of orotate with acquisition of a solvent deuterium from the putative general acid/base cysteine 133. As a result, the NMR spectra simplify from two sets of doublet of doublets to a singlet as the Pro-S proton on C5 of orotate is isolated from adjacent abundant coupling nuclei. Correlation with the PDB 1EP2 structure for the LlDHODB•orotate complex indicates positionally that the Pro-S hydrogen is available for exchange.² When NADH is incubated with the FMN subunit dimer, no enrichment of deuterium for either C4 stereochemical position is observed (Figure 4B). The NMR signal assignment for NADH was based on similar studies of glutathione/ thioredoxin reductase where the stereochemistry for NADPH oxidation was established from an X-ray crystal structure of the NADPH complex of that enzyme. 17,18 However, when NADH is incubated with native LIDHODB, both the Pro-R and Pro-S hydrogens are exchanged for solvent deuteriums, indicating that hydride exchange with NADH occurs at only the FAD active site with preferred Pro-R stereochemical selection (Figure 4C). The PyrK subunit has a fold topology of the ferredoxin-NADPH reductase (FNR) family.² Preferential exchange of the Pro-R hydrogen of NADH at the FAD of DHODB is consistent with stereochemistry implied in the structure of NADP+ bound to the FNR from Pisum sativum (pea).¹⁹ The relative slow exchange at the NADH Pro-S position at the FAD suggests that the flipped nicotinamide binding mode is also possible in the DHODB•NADH complex.

Kinetics of the Transient-State Reductive Half-Reaction. The reductive half-reaction of DHODB was observed in transient-state by mixing LlDHODB with NADH under anaerobic conditions. The data obtained are similar to those described by Combe et al. 16 and Mohsen et al.²⁰ When observed at 450 nm, biphasic traces were obtained (Figure 5A). The data were fit analytically using a linear combination of two exponentials. The first phase was rapid and poorly represented with the data acquired (dead-time of the instrument is 1.2 ms). As such, these data were fit with extrapolation to the known $t_{\rm zero}$ absorption defined by the spectrum of the enzyme collected in the absence of ligands. Moreover, it should be noted that only the three highest NADH concentrations deliver pseudo-first-order reactant ratios and so this experiment provided only a descriptive characterization of the reductive half-reaction.

When the observed rate constants are plotted against the NADH concentration, a limiting rate constant for reduction of \sim 2,200 s⁻¹ and an apparent K_d for NADH of \sim 200 μ M are obtained. At concentrations of NADH in excess of the enzyme concentration, a second phase is observed that can be described by a rate constant of 2–3 s⁻¹. This phase has a similar amplitude to the first at high concentrations of NADH but shows no distinct evidence of a dependence on the concentration of NADH. The origin of the second phase was investigated by repeating the reductive half-reaction in the presence of DHO to occupy the FMN active site (Figure 5A inset). The data obtained reveal less delineation as a result of

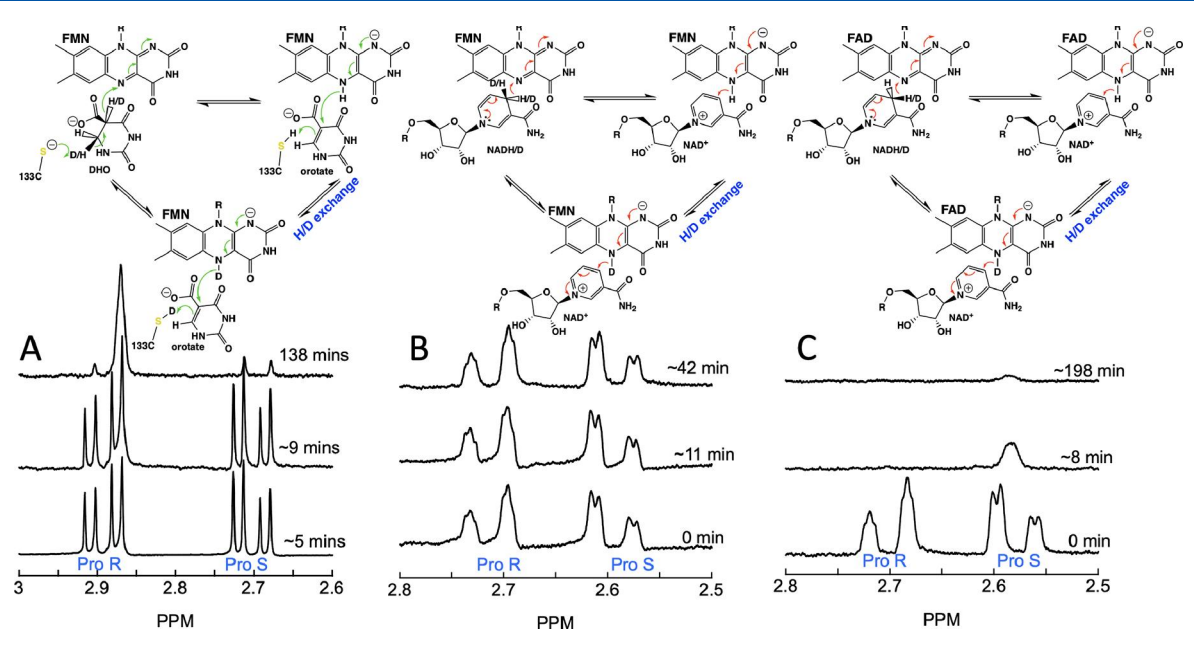


Figure 4. Evidence for reversible stereospecific hydride exchange at both DHODB flavins. (A) FMN subunit (5 μ M) was combined with 1 mM DHO under near anaerobic conditions. (B) FMN subunit (5 μ M) was combined with 1 mM NADH under near anaerobic conditions. (C) DHODB (5 μ M) was combined with 1 mM NADH under near anaerobic conditions. For each, ¹H NMR spectra derived from 32 (A, B) or 16 (C) FIDS were recorded at the times indicated. For DHO, stereochemical assignment is based on the PDB 1EP2 structure that includes bound orotate. Stereochemical assignment for NADH is drawn from the 2 × 99 structure of thioredoxin/glutathione reductase based on a similar analysis in ref 17.

increasing the rate constant for the second phase. The overall amplitude change in the presence of NADH and DHO is equivalent to that observed for both phases in the absence of DHO and suggests that four-electron reduction via the FAD active site alone can occur when NADH is supplied in excess of the enzyme concentration. In addition, it can be concluded that the rate of the second hydride transfer to the FAD to form the four-electron reduced state is increased as a result of DHO acting as an effector for reduction by NADH at the FAD. A priori, such an argument dictates that the initial two electrons from NADH reside on the FMN cofactor such that the FAD is returned to the oxidized state and available to receive two additional electrons.

Roughly coincident ($\sim 300 \text{ s}^{-1}$) with the first phase observed for flavin reduction, a rapid increase in absorption centered around 600 nm is observed. This species is, however, sustained throughout both phases of the reductive half-reaction and decays slowly with a catalytically irrelevant rate constant of $\sim 0.25 \text{ s}^{-1}$. To ascertain the origin of this absorption, CCD data sets collected for the reductive half-reaction were deconvoluted by fitting to a two-step irreversible model to yield the spectra for the individual states delineated by the observed rate constants (Figure 5C). Subtracting the spectrum of the prior species from the subsequent for the two phases observed yielded difference spectra that illustrate the absorption changes that occur in each phase. In Figure 5D, these difference spectra are compared to standard difference spectra for reduction of a flavin and oxidation of NADH. The absorption changes associated with the first phase clearly indicate reduction of flavin cofactor(s) apparently without clear additive contributions for NADH oxidation (see below). The extent of reduction defined by the change in extinction coefficient suggests reduction of ~1.2 flavins per DHODB heterodimer in the first event. Arising in this phase is the long wavelength absorption centered around 600 nm. This feature is not characteristic for NAD/flavin charge transfer absorption as it

has both relative intense absorption and has multiple absorption transitions. The interpretation was that this is accumulation of the blue form of flavin semiquinone(s) that arises with sequential one-electron transmission across the DHODB protein as first proposed by Combe et al. 16 This assertion also accounts for the lack of negative extinction coefficient changes indicative of NADH oxidation in the first difference spectrum as semiquinones typically have prominent absorption across the 320-380 nm region that are at least as intense as those for NADH.²¹ The second phase has less amplitude for flavin reduction than observed in the first phase, which is expected for the NADH concentration used in the CCD experiment based on what was observed for the amplitude dependence in the single wavelength data (Figure 5A). Also, this event does not result in added accumulation of the long-wavelength species. Together, the two phases observed sum to approximately the extinction coefficient change expected for two flavins reduced per subunit.

To define the identity of the long wavelength species, the reductive half-reaction was repeated using a limiting concentration of NADH (Figure 6). The CCD data obtained were fit to a model that assumes a quasi-equilibrium accumulation of reduced states, such that the two electrons from NADH are rapidly transmitted through the protein to the FMN, similar to what was recently established for mammalian and bacterial DPD. 13,22,23 However, the model employed included reduction of the FAD by NADH, two rapid (modeled as 10,000 s⁻¹) one-electron transmissions to reduce the FMN and rapid back flow for the second one-electron transfer (modeled as 2000 s⁻¹) permitting equilibrium accumulation of a flavin bisemiquinone state (as shown in Figure 6A). The choice of rapid rates for the steps that form and consume the bisemiquinone state was intended to force rapid equilibrium based on the rate for flavin reduction at 452 nm being the same as that for bisemiquinone accumulation at 600 nm (Figure 5B). Deconvolution using such a model fit to reveal the

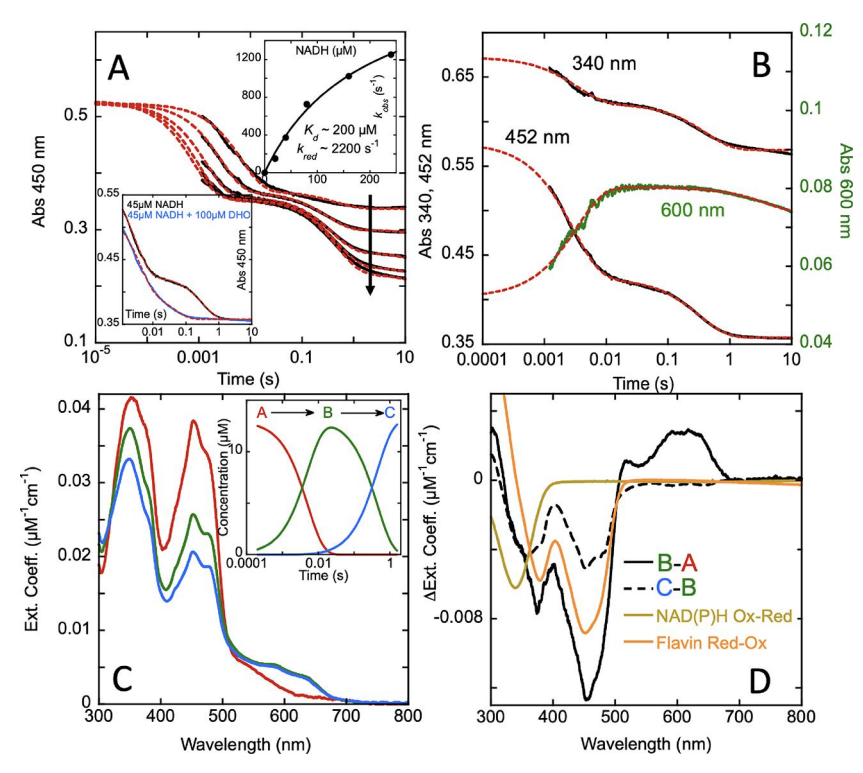


Figure 5. Transient-state reductive half-reaction for DHODB. (A) DHODB (15 μ M) was mixed with varied NADH concentrations (20, 40, 80, 160, 240 μ M) under anaerobic conditions and the reaction was observed at 450 nm. The arrow indicates increasing NADH concentration. The data were fit to a linear combination of two exponentials according to eq 2 and the first amplitude was defined by the measured t_{zero} absorbance at this wavelength. Note the third slow phase was not fit for these data. Upper inset depicts the dependence of the observed rate constant for the first phase on NADH concentration fit to the Adair equation (eq 4). Lower inset shows suppression of the second reduction phase when 18.7 μ M DHOD B was mixed with 45 μ M NADH in the presence and absence of 100 μ M DHO. (B) DHOD B (19 μ M) was mixed with NADH (45 μ M) under anaerobic conditions and the reaction was observed at 340, 450, and 600 nm. The data were fit to a linear combination of two exponentials according to eq 2. (C, D) Data collected using CCD detection. In this experiment DHOD B (13.5 μ M) was mixed with NADH (41 μ M) under anaerobic conditions and the reaction was observed at all wavelengths between 300 and 800 nm. Data were collected for 1.6 s with logarithmic spacing between spectra. (C) Deconvoluted spectra from a fit to a model that includes two sequential irreversible steps (A \rightarrow B \rightarrow C). Inset depicts the concentration profile derived from the fit. (D) Difference spectra obtained by subtracting spectrum A from B and spectrum B from C overlaid with standard spectra for flavin reduction (orange) and NADH oxidation (goldenrod).

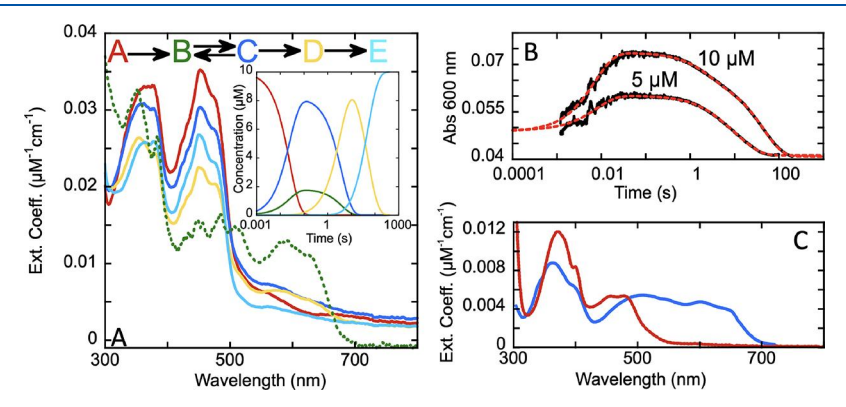


Figure 6. Transient state reductive half-reaction for DHODB with limiting NADH. (A) Deconvoluted spectra for the reaction of 17.5 μ M DHODB with 10 μ M NADH. CCD data were collected for two time frames (0.0016–1.6 s, 0.0016–793 s) and spliced together at the limit of the shorter. The three-dimensional data set was then fit to a four-step model where the second step was both rapid and reversible (k_f / k_r = 4.5) using SVD to yield spectra. Spectra were then corrected for the fraction of enzyme engaged in the reaction (57%). (B) Formation and decay of the semiquinones. 17 μ M DHODB with 5 and 10 μ M NADH and fit to three exponential terms according to eq 2. (C) Reference spectra for blue and red flavin semiquinones from ref 20 .

spectrum of the long wavelength transient-state species at all wavelengths acquired. This species has limited accumulation and so likely has error for the derived extinction coefficient(s) but the shape of its absorption spectrum closely resembles a combination of blue and red semiquinones (compare Figure

6A and 6C). Deconvolution to reveal this state is somewhat counterintuitive given that the reduction of the enzyme is within error concomitant with accumulation of the proposed bisemiquinone (Figure 5B–D). That this distinctive spectrum is unveiled by SVD suggests that the initial two-electron

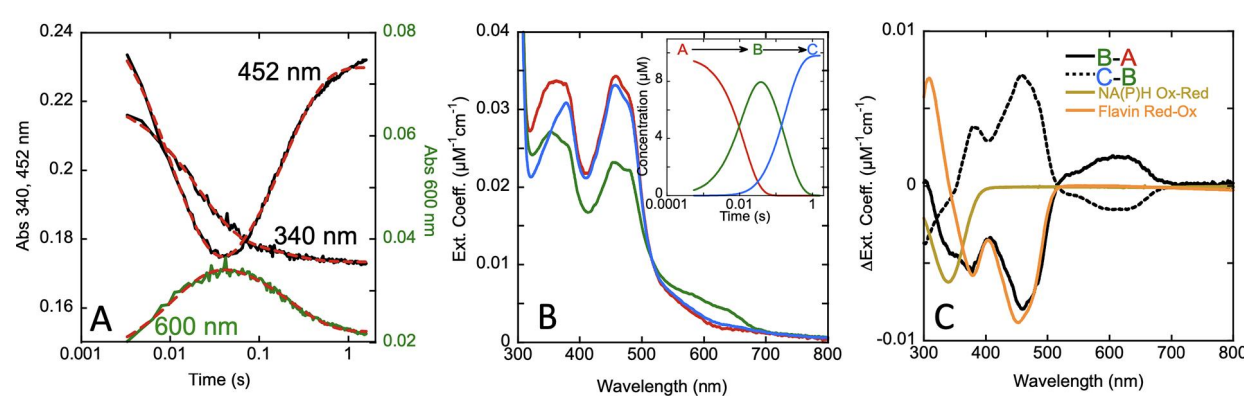


Figure 7. Transient-state single turnover for DHODB. DHODB (8.3 μ M) was mixed with NADH (10 μ M) and 240 μ M orotate under anaerobic conditions, and the reaction was observed using CCD detection for all wavelengths between 300 and 800 nm. Data were collected for 1.6 s with logarithmic spacing between spectra. (A) Extracted slices at indicated wavelengths fit to a linear combination of two exponentials according to eq 2. The 600 nm trace was repositioned for clarity by adding 0.13 AU. (B) Three-dimensional data sets of spectra were fit to a model that includes two sequential irreversible steps (A \rightarrow B \rightarrow C). Inset depicts the concentration profile derived from the fit. (C) Difference spectra obtained by subtracting spectrum A from B and spectrum B from C overlaid with standard spectra from flavin reduction (orange) and NAD(P)H oxidation (goldenrod).

reduction of the enzyme that reduces one of the two flavins to the hydroquinone state occurs with a slightly different rate than the rate of semiquinone accumulation. The observation of this species verifies the sequential one-electron transfer through the protein with concomitant accumulation of oneelectron reduced states of the flavins. However, one notable inconsistency is that the four-electron reduction described for Figure 5 should result in decay of the bisemiquinone state, but instead this feature persists. This apparent contradiction was also observed in the data presented by Combe et al. 16 and remains unexplained in the analysis presented here. Nonetheless, the bisemiquinone state is clearly a fractional component of the catalytic intermediate observed in single turnover (see Figure 7 below). The spectra also suggest that a reduced state of the Fe₂S₂ center accumulates. The final deconvoluted spectrum (teal spectrum in Figure 6A) has less absorption at ~550 nm arising from the iron-sulfur center (Figure 2B), suggesting that some fraction of the Fe₂S₂ center either becomes reduced or decomposes given sufficient time. However, it should be noted that the rate constants for the latter two events observed do not occur with rates sufficient to sustain catalysis. Moreover, it is not clear why the proposed bisemiquinone form slowly decays returning a fraction of the flavins to the oxidized state (compare yellow and teal spectra in Figure 6A and traces shown in Figure 6B).

Kinetics of Single Turnover Reactions Limited in NADH Concentration. Approximate single turnover reactions of LIDHODB were carried out by mixing the enzyme with near equimolar NADH and saturating orotate under anaerobic conditions. Data were collected using single wavelength photomultiplier detection and CCD (Figure 7). The single wavelength data obtained at 340, 452, and 600 nm were fit analytically to two events according to eq 2 to yield observed rate constants of ~ 80 and ~ 5 s⁻¹ (Figure 7A). Deconvoluted SVD-derived spectra determined by fitting CCD data sets for the same reactant ratios to two events returned similar rate constants (70 s⁻¹, 5.5 s⁻¹). The 5 s⁻¹ phase is \sim 3fold slower than the measured turnover number for the orotate reduction reaction direction (Table 1). This discrepancy is not accounted for in the data presented nor is it a function of higher order oligomeric states encountered with the elevated enzyme concentrations used in transient-state experiments

(Figure S4). The spectra indicate that the first phase involves reduction of one flavin cofactor and concomitant accumulation of a fractional bisemiquinone state (Figure 7B,C).

The second phase largely mirrors the first returning the enzyme to the oxidized state with concomitant decay of the bisemiquinone absorption transitions. Presumably, the second phase is reduction of the pyrimidine substrate and this assumption is addressed in the subsequent rapid quench product analysis section below. It is proposed that these data report reduction of the FAD cofactor being rate-limiting in the reductive half-reaction followed by two rapid single-electron transmission steps that reduce the FMN. Reversibility in the second single electron transmission results in the partial accumulation of an intervening bisemiquinone state identified in Figure 6. Given that the reduction reaction is fast compared to the reoxidation phase, high accumulation of the twoelectron reduced state is expected (Figure 7B inset) and the subsequent relative slow pyrimidine reduction phase promotes near maximal fractional bisemiquinone accumulation albeit to a limit of ~20% of all species. Assuming the rates of forward and reverse electron transfer vastly exceed the rate of hydride transfer in pyrimidine reduction, this phenomenon also accounts for why the decay of the bisemiquinone is concomitant with reoxidation of the enzyme. An estimation of the extent of reversibility can be made from the amplitude change at ~550 nm relative to the reported extinction coefficient of blue semiquinone states of 4,200 M⁻¹cm⁻¹.²⁴ The data suggest ~20% accumulation of the bisemiquinone state defining a ratio of ~4.5 for the relative forward and reverse electron transmission events for the second electron derived from NADH.

Transient-State Rapid Quench. The deconvoluted spectra for the reductive and oxidative steps observed in single turnover require time-dependent reaction composition analysis to confidently assign the chemistry occurring in each phase. The consumption of NADH and production of DHO in single turnover was monitored using single turnover rapid-mixing acid quench under anaerobic conditions preceding reverse phase HPLC analysis. The observation was based on accumulation of NAD⁺ and depletion of orotate, the former being the only stable NAD state in acid, and the latter, the pyrimidine form that has sufficient absorption to reliably

quantitate by HPLC (Figure 8). Broadly, the data obtained indicate that NADH is oxidized in the first phase observed in

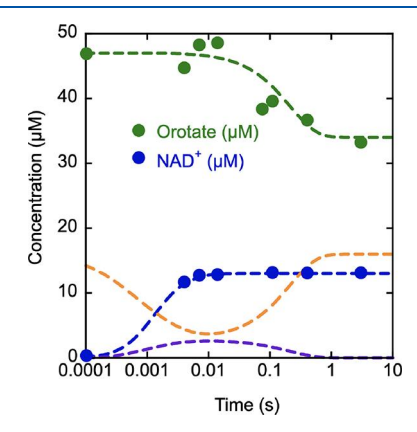


Figure 8. Rapid acid quench HPLC analysis of DHOD B single turnover reaction with orotate and limiting NADH. DHOD B (16 μ M) was mixed with NADH (13 μ M) and orotate (47 μ M) under anaerobic conditions. Reactions were quenched with 1 M TCA and 3 mM EDTA. Both NAD+ (blue circles) and orotate (green circles) quench data are overlaid with a single turnover reaction simulation (dashed lines) based on the catalytic steps and rate constants shown in Figure 9. The orotate depletion simulation (green) is based on all enzyme forms with orotate bound and free orotate and similarly the NAD+ accumulation (blue) is based on all enzyme forms with NAD+ bound and free NAD+. Also overlaid are the simulated decay and reformation of all states of the oxidized enzyme (orange) and the semiquinones (purple).

single turnover reactions and that orotate is consumed in the second phase observed; these data thus confirm the phase assignments made for the data depicted in Figure 7. The data were simulated (as opposed to fit) according to the model shown in Figure 9 and the concentration profiles shown with the data are derived from the model to illustrate (as opposed to offer evidence for) the proposed mechanism. The fractional accumulation of the bisemiquinone state is shown in purple and demonstrate the effect of reversibility in the second electron transfer step. Interestingly, the data cannot be simulated if the K_d for NADH determined in the reductive half-reaction (\sim 200 μ M, Figure 5A inset) is incorporated. Only when a dissociation constant for the DHODB•NADH complex of \sim <10 μM is built into the model does the simulated rate of oxidation of NADH conform to the data. This qualitatively suggests that orotate bound adjacent to the FMN cofactor acts as an effector for the binding of NADH at the FAD. Importantly, the change in concentration for both NAD+ and orotate matches the limiting concentration of NADH used in the reaction.

DISCUSSION

Dihydroorotate dehydrogenase 1B has an architecture that physically separates the two hydride transfer reactions required for the chemistry catalyzed. This arrangement of cofactors is reminiscent of the cofactor set found in dihydropyrimidine dehydrogenase (DPD). For both enzymes, the intervening iron sulfur center(s) dictate that two one-electron transfers are required to transmit the electrons between active sites. Despite extensive characterization, single-electron reduced states of the flavins have not been observed in transient-state analyses of DPD. ^{13,22,25} Here, we show fractional accumulation of both blue and red semiquinone forms in the orotate reduction

reaction of DHODB and propose that the relative low accumulation is a consequence of reversibility in the second electron transfer event.

Despite that the biochemical role of the DHOD reaction is pyrimidine biosynthesis, the orotate reduction reaction is favored ~9-fold over the NAD+ reduction reaction (Table 1, Figure S2). It was for this reason that the kinetics of orotate reduction were the subject of this investigation. The transientstate reductive half-reaction data reveal multiphasic flavin reduction steps (Figure 5). Logical dissection of these data is made challenging by the similarity of the absorption spectra for the flavin cofactors. The rate of the first phase is rapid and titrates with NADH concentration (Figure 5A). We tentatively assign this phase as reduction of the FMN cofactor. The basis for this assignment is that the second phase observed in the reductive half-reaction also results in flavin reduction and, on the basis of the additive extinction coefficient changes, brings the enzyme to the four-electron reduced state (Figure 5D). Presumably, this is only possible if the FAD were returned to the oxidized state in the first phase by delivering both electrons to the FMN cofactor. The addition of DHO in the reductive half-reaction eliminates the distinctly biphasic character but does not change the overall amplitude, suggesting that pyrimidines act as effectors accelerating acquisition of the second hydride from NADH such that four-electron reduction is largely monophasic. The proposal that the initial phase observed in the reductive half-reaction results in FMN reduction is entwined with the associated conclusion that it is the second one-electron transfer from the FAD cofactor that exhibits reversibility causing fractional accumulation of a bisemiquinone state (Figure 9). Furthermore, the sustained accumulation of the bisemiquinone state observed in the reductive half-reaction is consistent with, but not evidence for, a rapidly reversible second electron transfer for reduction of the FMN cofactor (Figures 5B and 6B).

A separate reductive half-reaction experiment using excess concentration of DHODB relative to NADH was performed in an attempt to better approximate first-order conditions and promote accumulation of the proposed bisemiquinone and thus capture using SVD the spectrum of this state across the wavelength range of the CCD detector (Figure 6). These data were modeled by building in reversibility for the second electron transfer step and the extinction coefficient of component spectrum for the bisemiquinone was sensitive to the ratio of forward and reverse rate constants defined for this step in the model. Also, since the actual fraction of accumulation of the bisemiquinone state is not known, the spectrum obtained for this state is unlikely to report actual extinction coefficients. Nonetheless, the spectrum returned is a good facsimile in terms of shape to the additive absorption contributions for red and blue flavin semiquinone states (Figure 6A). However, it should be noted that no evidence is offered that ties a semiquinone form to a specific flavin form.

Single turnover reactions were examined using both spectrophotometric methods and rapid quench. These experiments were limited by the concentration of NADH and orotate was added in excess to saturation as defined by the measured dissociation constant (Figure 3). These data are described by two events. The first event results in reduction of one flavin per DHODB heterodimer and, in terms of the difference spectrum, the second mirrors the first returning the enzyme to the oxidized state (Figure 7). These phases were definitively assigned using rapid quench and HPLC analysis as involving

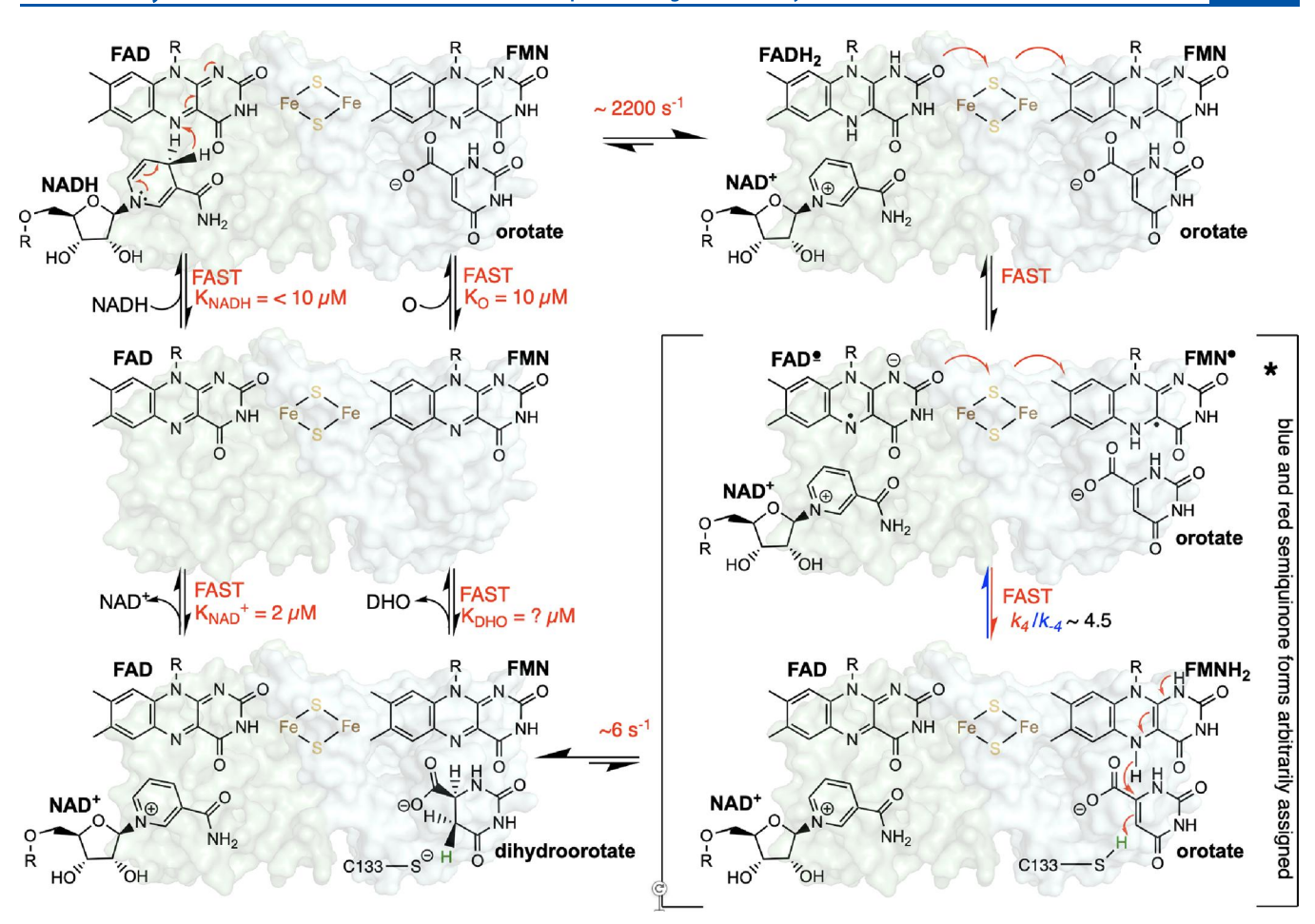


Figure 9. Proposed catalytic sequence of DHODB. Boxed state(s) represents single turnover intermediate shown in Figure 7. * represents the bisemiquinone state in which the blue and red semiquinone forms were arbitrarily assigned. Note: the options for binding and release/exchange of substrates shown are not comprehensive.

two-electron uptake from NADH followed by pyrimidine reduction (Figure 8). The proposed bisemiquinone accumulates concomitantly with the first phase and decays concomitantly with the reoxidation phase. Our conclusion of equilibrium accumulation of the bisemiquinone is compatible with these observations, the first phase resulting in FMN reduction via the FAD and the second phase draws these electrons out of the enzyme, simultaneously depleting the equilibrium accumulation of the flavin bisemiquinone.

CONCLUSIONS

DHODB and DPD are the only known flavin-dependent dehydrogenases that have evolved to have separate active sites for each hydride transfer event. Flavin-dependent dehydrogenases more often have a single active site that interacts with both reductant and oxidant substrates. For both enzymes, intervening iron sulfur clusters force the involvement of two one-electron transmissions per turnover, dictating that flavin semiquinones must form in catalysis. The data presented here are the first comprehensive analysis of these one-electron reduced states in these enzymes, which, while hardly unexpected, settles what was hitherto only presumed for these enzymes. In the case of DHODB, this observation was aided by rapid electron transmission and relative slow pyrimidine reduction that provided a window for equilibrium accumulation of the bisemiquinone state.

I ASSOCIATED CONTENT

5 Supporting Information

The Supporting Information is available free of charge at https://pubs.acs.org/doi/10.1021/acs.biochem.4c00025.

Figure S1: anion exchange separation of LIDHODB expression components; Figure S2: calibrated size exclusion of DHODB expression products; Figure S3: evidence of DHOD B reaction equilibrium under anaerobic conditions; Figure S4: dependence of the apparent turnover number on the concentration of LIDHODB (PDF)

AUTHOR INFORMATION

Corresponding Author

Graham R. Moran – Department of Chemistry and Biochemistry, Loyola University Chicago, Chicago, Illinois 60660, United States; ⊙ orcid.org/0000-0002-6807-1302; Phone: (773)508-3756; Email: gmoran3@luc.edu

Author

Corine O. Smith – Department of Chemistry and Biochemistry, Loyola University Chicago, Chicago, Illinois 60660, United States

Complete contact information is available at: https://pubs.acs.org/10.1021/acs.biochem.4c00025

Notes

The authors declare no competing financial interest. Lactoccocus lactis dihydroorotate dehydrogenase pyrK subunit: Q9CFW7. Lactoccocus lactis dihydroorotate dehydrogenase pyrDB subunit: Q9CFW8.

ACKNOWLEDGMENTS

This research was supported by National Science Foundation Grant CHE 2203593 to G.R.M.

REFERENCES

- (1) Nielsen, F. S.; Andersen, P. S.; Jensen, K. F. The B form of dihydroorotate dehydrogenase from Lactococcus lactis consists of two different subunits, encoded by the pyrDb and pyrK genes, and contains FMN, FAD, and [FeS] redox centers. *J. Biol. Chem.* 1996, 271, 29359–29365.
- (2) Rowland, P.; Norager, S.; Jensen, K. F.; Larsen, S. Structure of dihydroorotate dehydrogenase B: electron transfer between two flavin groups bridged by an iron-sulphur cluster. *Structure* **2000**, *8*, 1227—1238.
- (3) Dobritzsch, D.; Ricagno, S.; Schneider, G.; Schnackerz, K. D.; Lindqvist, Y. Crystal structure of the productive ternary complex of dihydropyrimidine dehydrogenase with NADPH and 5-iodouracil. Implications for mechanism of inhibition and electron transfer. *J. Biol. Chem.* **2002**, 277, 13155–13166.
- (4) Dobritzsch, D.; Schneider, G.; Schnackerz, K. D.; Lindqvist, Y. Crystal structure of dihydropyrimidine dehydrogenase, a major determinant of the pharmacokinetics of the anti-cancer drug 5-fluorouracil. *EMBO J.* **2001**, *20*, 650–660.
- (5) Bjornberg, O.; Rowland, P.; Larsen, S.; Jensen, K. F. Active site of dihydroorotate dehydrogenase A from Lactococcus lactis investigated by chemical modification and mutagenesis. *Biochemistry* **1997**, *36*, 16197–16205.
- (6) Winer, A. D. Crystallization of Nicotinamide Adenine Dinucleotide. *J. Biol. Chem.* **1964**, 239, PC3598.
- (7) Horecker, B. L.; Kornberg, A. The extinction coefficients of the reduced band of pyridine nucleotides. *J. Biol. Chem.* **1948**, *175*, 385–390
- (8) Beaupre, B. A.; Roman, J. V.; Moran, G. R. An improved method for the expression and purification of porcine dihydropyrimidine dehydrogenase. *Protein Expr Purif* **2020**, *171*, No. 105610.
- (9) Hoyle, W. C.; Benga, J. 2,4,6-tris2'[4'-(p-sulfophenyl)pyridyl]-striazine: a new analytical reagent for the spectrophotometric determination of iron. *Talanta* 1980, 27, 963–969.
- (10) Hedayati, M.; Abubaker-Sharif, B.; Khattab, M.; Razavi, A.; Mohammed, I.; Nejad, A.; Wabler, M.; Zhou, H.; Mihalic, J.; Gruettner, C.; DeWeese, T.; Ivkov, R. An optimized spectrophotometric assay for convenient and accurate quantitation of intracellular iron from iron oxide nanoparticles. *Int. J. Hyperthermia* **2018**, 34, 373–381.
- (11) Smith, F. E.; Herbert, J.; Gaudin, J.; Hennessy, D. J.; Reid, G. R. Serum iron determination using ferene triazine. *Clin Biochem* **1984**, *17*, 306–310.
- (12) Moran, G. R. Anaerobic methods for the transient-state study of flavoproteins: The use of specialized glassware to define the concentration of dioxygen. *Methods Enzymol* **2019**, *620*, 27–49.
- (13) Beaupre, B. A.; Forouzesh, D. C.; Moran, G. R. Transient-State Analysis of Porcine Dihydropyrimidine Dehydrogenase Reveals Reductive Activation by NADPH. *Biochemistry* **2020**, *59*, 2419–2431.
- (14) Argyrou, A.; Washabaugh, M. W.; Pickart, C. M. Dihydroorotate dehydrogenase from Clostridium oroticum is a class 1B enzyme and utilizes a concerted mechanism of catalysis. *Biochemistry* **2000**, *39*, 10373–10384.
- (15) Marcinkeviciene, J.; Jiang, W.; Locke, G.; Kopcho, L. M.; Rogers, M. J.; Copeland, R. A. A second dihydroorotate dehydrogenase (Type A) of the human pathogen Enterococcus faecalis: expression, purification, and steady-state kinetic mechanism. *Arch. Biochem. Biophys.* **2000**, *377*, 178–186.

- (16) Combe, J. P.; Basran, J.; Hothi, P.; Leys, D.; Rigby, S. E.; Munro, A. W.; Scrutton, N. S. Lys-D48 is required for charge stabilization, rapid flavin reduction, and internal electron transfer in the catalytic cycle of dihydroorotate dehydrogenase B of Lactococcus lactis. *J. Biol. Chem.* **2006**, 281, 17977—17988.
- (17) Smith, M. M.; Moran, G. R. Assigning function to active site residues of Schistosoma mansoni thioredoxin/glutathione reductase from analysis of transient state reductive half-reactions with variant forms of the enzyme. *Front. Mol. Biosci.* **2023**, *10*, 1258333.
- (18) Angelucci, F.; Dimastrogiovanni, D.; Boumis, G.; Brunori, M.; Miele, A. E.; Saccoccia, F.; Bellelli, A. Mapping the catalytic cycle of Schistosoma mansoni thioredoxin glutathione reductase by X-ray crystallography. *J. Biol. Chem.* **2010**, 285, 32557–32567.
- (19) Deng, Z.; Aliverti, A.; Zanetti, G.; Arakaki, A. K.; Ottado, J.; Orellano, E. G.; Calcaterra, N. B.; Ceccarelli, E. A.; Carrillo, N.; Karplus, P. A. A productive NADP+ binding mode of ferredoxin-NADP+ reductase revealed by protein engineering and crystallographic studies. *Nat. Struct. Biol.* 1999, 6, 847–853.
- (20) Mohsen, A. W.; Rigby, S. E.; Jensen, K. F.; Munro, A. W.; Scrutton, N. S. Thermodynamic basis of electron transfer in dihydroorotate dehydrogenase B from Lactococcus lactis: analysis by potentiometry, EPR spectroscopy, and ENDOR spectroscopy. *Biochemistry* **2004**, *43*, 6498–6510.
- (21) Crozier-Reabe, K.; Moran, G. R. Form follows function: structural and catalytic variation in the class a flavoprotein monoxygenases. *Int. J. Mol. Sci.* **2012**, *13*, 15601–15639.
- (22) Beaupre, B. A.; Forouzesh, D. C.; Butrin, A.; Liu, D.; Moran, G. R. Perturbing the Movement of Hydrogens to Delineate and Assign Events in the Reductive Activation and Turnover of Porcine Dihydropyrimidine Dehydrogenase. *Biochemistry* **2021**, *60*, 1764–1775.
- (23) Smith, M. M.; Forouzesh, D. C.; Kaley, N. E.; Liu, D.; Moran, G. R. Mammalian dihydropyrimidine dehydrogenase: Added mechanistic details from transient-state analysis of charge transfer complexes. *Arch. Biochem. Biophys.* **2023**, 736, No. 109517.
- (24) Collins, H. F.; Biedendieck, R.; Leech, H. K.; Gray, M.; Escalante-Semerena, J. C.; McLean, K. J.; Munro, A. W.; Rigby, S. E. J.; Warren, M. J.; Lawrence, A. D. Bacillus megaterium Has Both a Functional BluB Protein Required for DMB Synthesis and a Related Flavoprotein That Forms a Stable Radical Species. *PLoS One* **2013**, *8*, e55708 DOI: 10.1371/journal.pone.0055708.
- (25) Smith, M. M.; Moran, G. R. The unusual chemical sequences of mammalian dihydropyrimidine dehydrogenase revealed by transient-state analysis. *Methods Enzymol* **2023**, *685*, 373–403.
- (26) Fagan, R. L.; Nelson, M. N.; Pagano, P. M.; Palfey, B. A. Mechanism of flavin reduction in class 2 dihydroorotate dehydrogenases. *Biochemistry* **2006**, *45*, 14926–14932.
- (27) Fagan, R. L.; Jensen, K. F.; Bjornberg, O.; Palfey, B. A. Mechanism of flavin reduction in the class 1A dihydroorotate dehydrogenase from Lactococcus lactis. *Biochemistry* **200**7, *46*, 4028–4036.
- (28) Nizam, S.; Verma, S.; Borah, N. N.; Gazara, R. K.; Verma, P. K. Comprehensive genome-wide analysis reveals different classes of enigmatic old yellow enzyme in fungi. *Sci. Rep.* **2014**, *4*, 4013.
- (29) Stott, K.; Saito, K.; Thiele, D. J.; Massey, V. Old Yellow Enzyme. The discovery of multiple isozymes and a family of related proteins. *J. Biol. Chem.* **1993**, *268*, 6097–6106.
- (30) Fu, G.; Yuan, H.; Wang, S.; Gadda, G.; Weber, I. T. Atomic-resolution structure of an N5 flavin adduct in D-arginine dehydrogenase. *Biochemistry* **2011**, *50*, 6292–6294.
- (31) Algov, I.; Grushka, J.; Zarivach, R.; Alfonta, L. Highly Efficient Flavin-Adenine Dinucleotide Glucose Dehydrogenase Fused to a Minimal Cytochrome C Domain. *J. Am. Chem. Soc.* **2017**, *139*, 17217–17220.